



2 Channelized melt flow in downwelling mantle: Implications for 3 ^{226}Ra - ^{210}Pb disequilibria in arc magmas

4 N. Petford,¹ M. A. Koenders,² and S. Turner³

5 Received 20 December 2007; revised 6 June 2008; accepted 27 August 2008; published XX Month 2008.

6 [1] We present the results of an analytical model of porous flow of viscous melt into
7 a steadily dilating “channel” (defined as a cluster of smaller veins) in downwelling subarc
8 mantle. The model predicts the pressure drop in the mantle wedge matrix surrounding
9 the channel needed to drive melt flow as a function of position and time. Melt is sucked
10 toward the dilatant region at a near-constant velocity (10^{-5} s^{-1}) until veins comprising
11 the channel stop opening ($t = \tau$). Fluid elements that complete their journey within the
12 time span $t < \tau$ arrive at a channel. Our results make it possible to calculate the region of
13 influence sampled by melt that surrounds the channel. This region is large compared to
14 the model size of the channelized region driving flow. For a baseline dilation time of
15 1 year and channel half width of 2 m, melt can be sampled over an 80-m radius and has
16 the opportunity to sample matrix material with potentially contrasting chemistry on
17 geologically short timescales. Our mechanical results are consistent with a downgoing arc
18 mantle wedge source region where melting and melt extraction by porous flow to a
19 channel network are sufficiently rapid to preserve source-derived ^{238}U - ^{230}Th - ^{226}Ra , and
20 potentially also ^{226}Ra - ^{210}Pb , disequilibria, prior to magma ascent to the surface. Since
21 this is the rate-determining step in the overall process, it allows the possibility that such
22 short-lived disequilibria measured in arc rocks at the surface are derived from deep in
23 the mantle wedge. Stresses due to partial melting do not appear capable of producing
24 the desired sucking effect, while the order of magnitude rate of shear required to drive
25 dilation of $\sim 10^{-7} \text{ s}^{-1}$ is much larger than values resulting from steady state subduction.
26 We conclude that local deformation rates in excess of background plate tectonic rates are
27 needed to “switch on” the dilatant channel network and to initiate the sucking effect.

28 **Citation:** Petford, N., M. A. Koenders, and S. Turner (2008), Channelized melt flow in downwelling mantle: Implications for
29 ^{226}Ra - ^{210}Pb disequilibria in arc magmas, *J. Geophys. Res.*, 113, XXXXXX, doi:10.1029/2007JB005563.

31 1. Introduction

32 [2] The dynamic behavior of the Earth is a result of its
33 internal heat. Volcanism provides the most spectacular
34 manifestation of this, and heat advection by magmas is
35 the most efficient means of heat transport. Beneath the
36 Earth’s volcanic mid-ocean ridges and oceanic islands,
37 melting occurs in an upwelling mantle matrix with melt
38 extraction often presumed to occur via percolative flow
39 followed by channeled flow [e.g., *Spiegelman et al.*, 2001;
40 *Spiegelman and Kelemen*, 2003]. Currently, the timescales
41 and length scales governing this important flow transition
42 are poorly known. Yet without some estimate of melt
43 velocities and transport times, the degree to which interac-
44 tion between melt and peridotite matrix may take place
45 remains speculative at best. U series disequilibria can be

used to constrain the rate of matrix upwelling and also the 46
threshold porosity at which melt is extracted from the 47
matrix. In contrast, the total time for melt extraction is 48
ambiguous depending on whether the observed disequilibria 49
are modeled by dynamic melting with rapid extraction 50
[e.g., *McKenzie*, 1985; *Williams and Gill*, 1989] or equi- 51
librium porous flow involving very slow melt percolation 52
[*Spiegelman and Elliott*, 1993; *Asimow and Stolper*, 1999]. 53
Because the exact melting rate and porosity are linked to the 54
total time involved, better knowledge of the timescales and 55
length scales of melt transport in the source region would 56
help improve estimates of these variables. Nevertheless, 57
there is growing evidence that melt extraction beneath ridges 58
and ocean island volcanoes is fast and may in some cases 59
take place on decadal timescales [*Bourdon et al.*, 2005; 60
Rubin et al., 2005a; *Stracke et al.*, 2006]. 61

[3] At island arcs the situation is rather different. Because 62
of induced convection against the subducting plate, most 63
current models of melt production in arcs assume that the 64
mantle wedge directly above the slab, where a significant 65
portion of arc magmas is generated, moves downward 66
through the melting zone. Furthermore, the ^{231}Pa disequi- 67
libria are consistent with the matrix flow rate in the melting 68
region being the same as the local convergence rates. 69

¹School of Conservation Sciences, Bournemouth University, Poole, UK.

²Centre for Earth and Environmental Science Research, Kingston University, Kingston, UK.

³GEMOC, Department of Earth and Planetary Sciences, Macquarie University, Sydney, New South Wales, Australia.

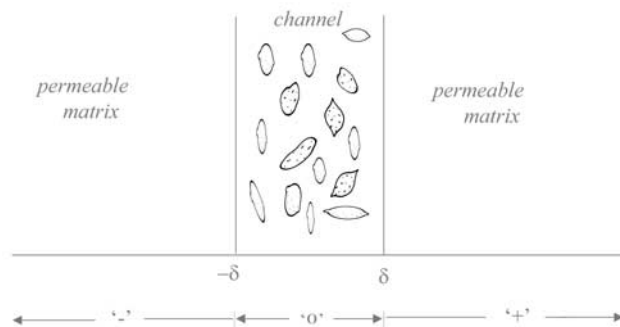


Figure 1. Geometry of the channel, defined as a high- porosity ($n = 0.4$) dilational zone comprising numerous smaller veins. Three regions are identified: 0, where the dilation occurs; plus, almost undeformable permeable material to the right of 0 at $x > \delta$; and minus, almost undeformable permeable material to the left of 0 at $x < -\delta$.

70 Although recent work suggests that decompression melting
 71 due to viscous entrainment may also take place in some arcs
 72 [Conder *et al.*, 2002], the problem of melt extraction in a
 73 downwelling matrix still requires attention. Additionally,
 74 ^{226}Ra excesses in arc lavas correlate with trace element
 75 indices of fluid addition (e.g., Sr/Th) and so are inferred to
 76 result from fluid addition from the subducting plate. Criti-
 77 cally, because this implies these signals originate at the base
 78 of the melt region, their preservation allows important
 79 constraints to be placed on the magma extraction rate, and
 80 this may be on the order of $100\text{--}1000\text{ m a}^{-1}$ [Turner *et al.*,
 81 2001]. Although porous flow models can also produce large
 82 ^{226}Ra excesses [Spiegelman and Elliott, 1993], they do not
 83 predict a positive correlation with Sr/Th.

84 [4] In contrast to creeping flow modeled successfully for
 85 mid-ocean ridges, these higher transport rates require
 86 channel-dominated melt ascent toward the surface. How-
 87 ever, an important condition remains, namely, that the melt is
 88 supplied to channels over some governing length scale fast
 89 enough that short-lived isotope disequilibria are preserved.
 90 Such high rates require a fluid dynamical explanation, yet
 91 they appear incompatible with a transport process governed
 92 purely by compaction and simple porous flow [e.g., Sleep,
 93 1988; Stevenson, 1989; Maaloe, 2005].

94 [5] Clearly, there is a need to develop physical models for
 95 melt transport in the mantle wedge above a subducting slab
 96 analogous to those put forward for melt extraction at mid-
 97 ocean ridges [e.g., Aharonov *et al.*, 1995; Spiegelman *et al.*,
 98 2001; Spiegelman and Kelemen, 2003], whereby an initially
 99 small melt fraction, distributed at or along grain boundaries,
 100 develops into a channelized network. More generally, in
 101 order to develop a self-consistent model of subduction
 102 zones, there is a need to explore physical processes that
 103 take place in the mantle wedge on short temporal and spatial
 104 scales [e.g., van Keken, 2003]. As a first step toward this
 105 goal, we present the initial results of an analytical study of
 106 melt flow in porous, downwelling arc mantle. We assume
 107 a simple 1-D geometry where melt flows radially toward a
 108 zone of reduced pressure, defined macroscopically as a
 109 linear channel of constant half width bounding a cluster of
 110 smaller veins that open incrementally over a fixed timescale.

From this, we seek as a first step to establish a rigorous 111
 solution to the mechanics of the problem and provide order 112
 of magnitude estimates of (1) the characteristic pressure 113
 gradients needed to drive porous flow of melt toward a 114
 dilating channel, (2) the maximum distance (or radius of 115
 influence) surrounding a dilating channel from which melt 116
 can be sampled such that a required activity ratio is pre- 117
 served, and (3) the possible mechanism(s) governing dilation 118
 in downwelling mantle. Once the theory part is established, 119
 the way is paved for further (numerical) work that can model 120
 the flow process in more detail. 121

2. Model Geometry and Assumptions 122

[6] The majority of U series evidence to date points to the 123
 need for some kind of channelized flow in the mantle [e.g., 124
 McKenzie, 1985; Turner *et al.*, 2001, 2003; Stracke *et al.*, 125
 2006]. Yet despite this, some element of porous flow must 126
 still prevail at the outset of the transport process [e.g., 127
 Spiegelman *et al.*, 2001]. Our goal at this stage is not to 128
 model channel formation itself but rather to show under 129
 what conditions melt flow will be fast enough to preserve 130
 isotopic disequilibrium in the source region (note we use 131
 “channel” here to describe some form of linear, dilatant 132
 feature as distinct from a brittle crack). 133

[7] A sketch of the simple geometry under investigation 134
 is shown in Figure 1. The model comprises a central region 135
 (or channel) that contains dilational structures or veins (for 136
 want of a better word). The half width of the channel δ is of 137
 the order of meters (we use a guideline number of $\delta = 2\text{ m}$ in 138
 our calculations), comparable with estimates from Takahashi 139
 [1992] of vein and channel structures in mantle rocks now 140
 preserved at the surface. The permeability in the dilating 141
 channel is much greater than that of the surrounding rock. In 142
 order to estimate its value, we employ the well-known 143
 Kozeny-Carman formula, which is normally used for 144
 granular materials. Let the length scale d between the 145
 veins comprising the channel be of the order of 10^{-2} m and 146
 the melt fraction (porosity) $n_0 = 0.2$, then the permeability in 147
 the region that is dominated by the vein system comes out as 148
 $\kappa_0 = d^2 n_0^3 / [150(1 - n_0)^3] \simeq 10^{-8}\text{ m}^2$; this value will be fixed 149
 arbitrarily as a guideline number to allow us to focus on the 150
 details of the process. The channel is surrounded by mantle 151
 with fixed lower permeability: $\kappa = 10^{-14}\text{ m}^2$. The conduc- 152
 tivities in the channel and surrounding rock related to 153
 the permeabilities through the viscosity η are $k_0 = \kappa_0/\eta$ 154
 and $k = \kappa/\eta$. 155

3. Flow Equations 156

[8] The melt density and viscosity remain constant during 157
 flow. We solve for the average pressure drop in the channel 158
 and recover the associated flow rate as melt is sucked 159
 toward it. Three regions are identified (Figure 1): “zero,” 160
 where the channel is located; “plus,” almost undeformable 161
 permeable material to the right of 0 at $x > \delta$; and “minus,” 162
 almost undeformable permeable material to the left of 0 at 163
 $x < -\delta$. The flow is driven by a strain that is ramped up to a 164
 value e_0 in a time τ . For $t > \tau$ the strain is kept constant at 165
 e_0 . The magma is compressible with compressibility β ; the 166
 porosities are n_0 in the channel and n in the surrounding 167
 rock. The fluid excess pressure is denoted by p . 168

t1.1 **Table 1.** Sensitivity Analysis Showing Effects of Changes to Variables Listed in Table 2

t1.2		Largest Distance (m)	Time to $x = 0$
t1.3	Value (see Table 2)	100	τ
t1.4	$\tau = 10^8$ s	100	τ
t1.5	$\delta = 4$ m	100	1.3τ
t1.6	$\beta = 10^{-9}$ Pa $^{-1}$	100	3τ
t1.7	$k = 10^{-10}$ m 2 Pa $^{-1}$ s $^{-1}$	100	τ
t1.8	$k_0 = 10^{-9}$ m 2 Pa $^{-1}$ s $^{-1}$	100	τ
t1.9	$e_0 = 0.05$	50	τ
t1.10	$n = 0.005$	25	1.1τ
t1.11	$n_0 = 0.4$	100	1.2τ

169 [9] Biot's equation reads

$$k_0 \frac{\partial^2 p}{\partial x^2} = n_0 \beta \frac{\partial p}{\partial t} + \frac{\partial e}{\partial t} \quad (-\delta < x < \delta) \quad (1)$$

170

$$k \frac{\partial^2 p}{\partial x^2} = n \beta \frac{\partial p}{\partial t} \quad (x > \delta, x < -\delta). \quad (2)$$

172 [10] The boundary conditions are

$$p(\delta - \varepsilon, t) = p(\delta + \varepsilon, t) \quad (\varepsilon \rightarrow 0), \quad (3)$$

175

$$p(-\delta - \varepsilon, t) = p(-\delta + \varepsilon, t) \quad (\varepsilon \rightarrow 0), \quad (4)$$

177

$$k_0 \frac{\partial p}{\partial x}(\delta - \varepsilon, t) = k \frac{\partial p}{\partial x}(\delta + \varepsilon, t) \quad (\varepsilon \rightarrow 0), \quad (5)$$

179

$$k_0 \frac{\partial p}{\partial x}(-\delta + \varepsilon, t) = k \frac{\partial p}{\partial x}(-\delta - \varepsilon, t) \quad (\varepsilon \rightarrow 0), \quad (6)$$

182

$$\frac{\partial p}{\partial x}(\pm L, t) = 0 \quad (L \rightarrow \infty). \quad (7)$$

185 [11] The solution is obtained by Laplace transform. Full
186 details are given in Appendix A. The solution of the
187 problem is given in terms of functions $\Psi_0(\zeta, t)$ and
188 $\Psi_1(\zeta, t)$; these depend on the time it takes for the veins
189 to open (τ). In Appendix A, their form is derived

$$\begin{aligned} \Psi_0(\zeta, t) = & -\frac{\zeta \sqrt{t} \exp\left(-\frac{\zeta^2}{4t}\right)}{\tau \sqrt{\pi}} \\ & + \frac{(2t + \zeta^2) \left[1 - \operatorname{erf}\left(\frac{\zeta}{2\sqrt{t}}\right)\right]}{\tau \sqrt{\pi}} \quad (t < \tau) \\ = & 1 + \frac{\zeta \left(\exp\left(\frac{-\zeta^2}{4(t-\tau)}\right) \sqrt{t-\tau} - \exp\left(\frac{-\zeta^2}{4t}\right) \sqrt{t}\right)}{\tau \sqrt{\pi}} \\ & \cdot \frac{(2t - 2\tau + \zeta^2) \operatorname{erf}\left(\frac{\zeta}{2\sqrt{t-\tau}}\right) - (2t + \zeta^2) \operatorname{erf}\left(\frac{\zeta}{2\sqrt{t}}\right)}{2\tau} \\ & \cdot (t > \tau) \end{aligned} \quad (8)$$

$$\begin{aligned} \Psi_1(\zeta, t) = & \frac{2\sqrt{t} \exp\left(-\frac{\zeta^2}{4t}\right)}{\tau \sqrt{\pi}} - \frac{\zeta \left[1 - \operatorname{erf}\left(\frac{\zeta}{2\sqrt{t}}\right)\right]}{\tau} \quad (t < \tau) \\ = & -\frac{2 \left(\exp\left(\frac{-\zeta^2}{4(t-\tau)}\right) \sqrt{t-\tau} - \exp\left(\frac{-\zeta^2}{4t}\right) \sqrt{t}\right)}{\tau \sqrt{\pi}} \\ & - \frac{\zeta \left[\operatorname{erf}\left(\frac{\zeta}{2\sqrt{t-\tau}}\right) - \operatorname{erf}\left(\frac{\zeta}{2\sqrt{t}}\right)\right]}{\tau} \quad (t > \tau). \end{aligned} \quad (9)$$

[12] The superficial velocity (that is, the fluid discharge
per unit time and area) of melt flowing toward the channel is
simply

$$v = -k \frac{\partial p}{\partial x}. \quad (10)$$

[13] For convenience, two parameters with the dimension
of $\sqrt{s} \text{ m}^{-1}$ are introduced: $\mu_0 = \sqrt{n_0 \beta / k_0}$ and $\mu = \sqrt{n \beta / k}$.
The pore pressure (as a function of position and time) due to
the opening vein in the region marked plus is

$$\begin{aligned} p(x, t) = & \frac{e_0 k_0 \mu_0}{\beta n_0 (k \mu + k_0 \mu_0)} \sum_{j=0}^{\infty} \left(\frac{-k \mu + k_0 \mu_0}{k \mu + k_0 \mu_0}\right)^j \\ & \cdot [\Psi_0(\mu(x - \delta) + 2(j+1)\mu_0 \delta, t) \\ & - \Psi_0(\mu(x - \delta) + 2j\mu_0 \delta, t)], \end{aligned} \quad (11)$$

and the superficial velocity turns out to be

$$\begin{aligned} v(x, t) = & -\frac{e_0 k k_0 \mu_0 \mu}{\beta n_0 (k \mu + k_0 \mu_0)} \sum_{j=0}^{\infty} \left(\frac{-k \mu + k_0 \mu_0}{k \mu + k_0 \mu_0}\right)^j \\ & \cdot [\Psi_1(\mu(x - \delta) + 2(j+1)\mu_0 \delta, t) \\ & - \Psi_1(\mu(x - \delta) + 2j\mu_0 \delta, t)]. \end{aligned} \quad (12)$$

[14] The corresponding actual melt velocity is $v(x, t)/n$.

4. Results

[15] Our primary aim here is to model the magnitude of
melt flow in response to pressure reductions associated with
the opening up of channels as defined in Figure 1 in the
mantle wedge (how the channels themselves might happen
to form is discussed in section 5). There is no simple scaling
in this problem as there are three length scales: $\lambda_1 = \mu_0^{-1}$
 $\sqrt{\tau}$, $\lambda_2 = \mu^{-1} \sqrt{\tau}$, and $\lambda_3 = \delta$. The timescales are to τ as well
as to the factors $\beta n_0 (k \mu + k_0 \mu_0) / (e_0 k k_0 \mu_0 \mu \lambda_i)$ ($i = 1, 2, 3$). So,
here it is important to have some idea of the variable range
for results to be presented. Naturally, there is an element of
speculation in the parameter values as no precise measure-
ments are available. In our simple model we take τ (dilation
time) as 1 year. This is arbitrary. Any other value of τ is, of
course, permitted (see section 4); examples include scaling
the channel opening time to a short-lived isotope half-life.
Relevant values are summarized in Table 1. To begin with,
the pressure as a function of position and time is obtained.
This is illustrated here for a choice of parameters (melt
viscosity, melt fraction, etc.) as given in Table 1 with the
exception of k , which is set to $10^{-10} \text{ Pa}^{-1} \text{ m}^2 \text{ s}^{-1}$; the
reason for the deviation of the permeability parameter is that
this choice results in rather smoother curves, which are

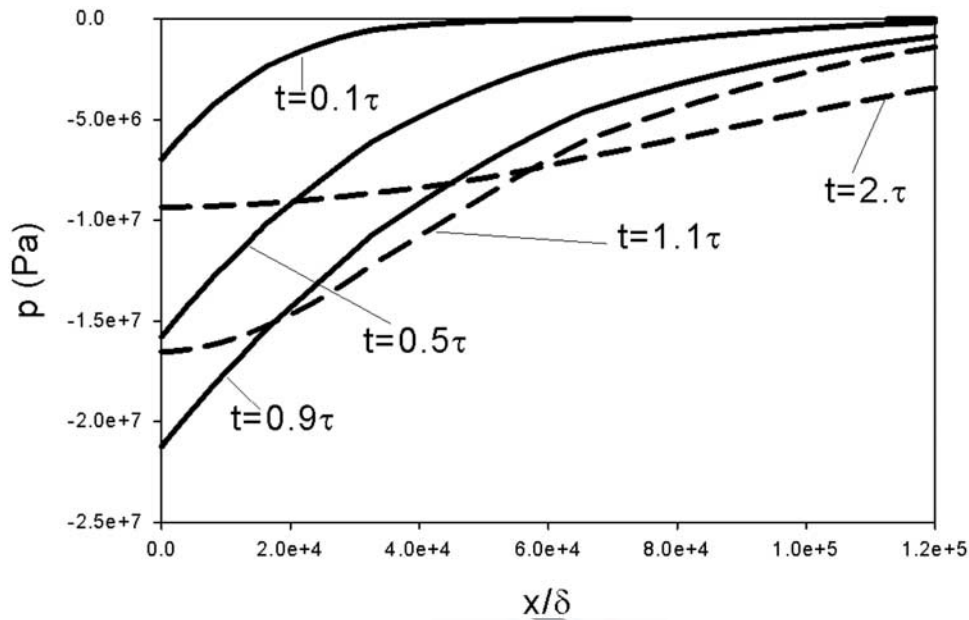


Figure 2. Pressure as a function of nondimensional position at various times (t). All parameters are as in Table 1 except $k = 10^{-10} \text{ Pa}^{-1} \text{ m}^2 \text{ s}^{-1}$. Solid lines show the pressure history as the channel is opening ($t < \tau$) and dashed lines show the pressure history where $t > \tau$. The behavior is such that after a short time the pressure settles back to a value close to initial. The pressure drop is, however, active over a wide area.

231 desirable for illustrative purposes. Figure 2 shows the
 232 pressure as a function of position in the plus region, plotted
 233 as a function of position (expressed in δ) at various times. It
 234 is seen that the pressure falls as the channels open up (a
 235 good analogy is that of drawing fluid into a syringe at a
 236 fixed rate) and that the region of influence is large compared

to the size of the channelized region. When the channel 237
 opening ceases (at $t = \tau$), the pressure rapidly returns to the 238
 equilibrium value $p = 0$ while the magnitude of the pressure 239
 gradient (and, thus, the fluid velocity) decreases. In the 240
 example here, the gradient is already negligible after $t = 2\tau$. 241
 This behavior is exactly as one would expect it. The 242

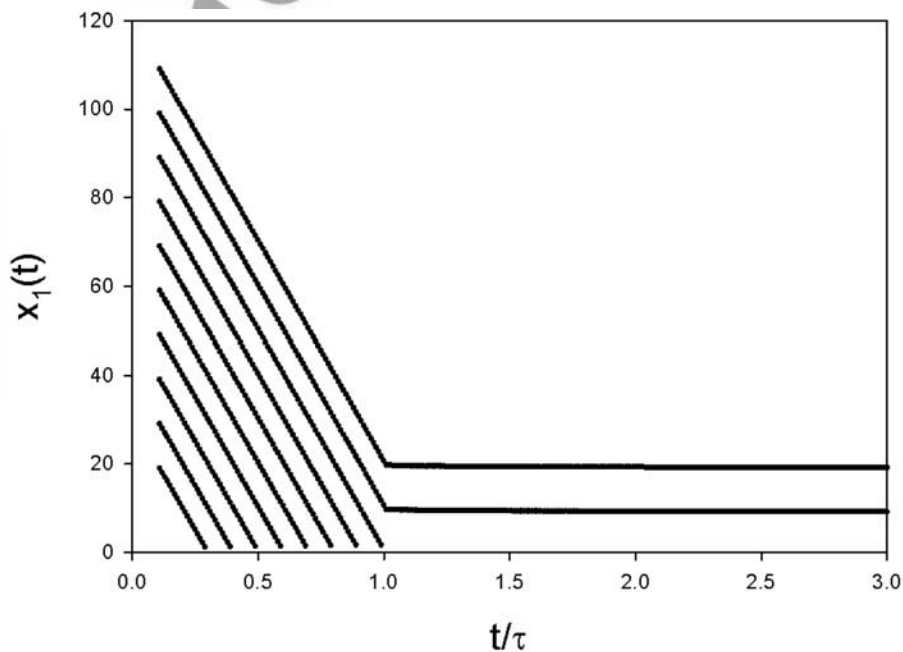


Figure 3. Trajectories of fluid elements for the parameter values in the Table 1. Melt is drawn toward the opening channel by pressure gradients set up as the channel widens over the period of 1 year, after which the pressure gradient is shut off. The channel is located at position $t/\tau = 1.0$. Fluid will reach this position from a distance $x_1(t)$ of up to 80 m away.

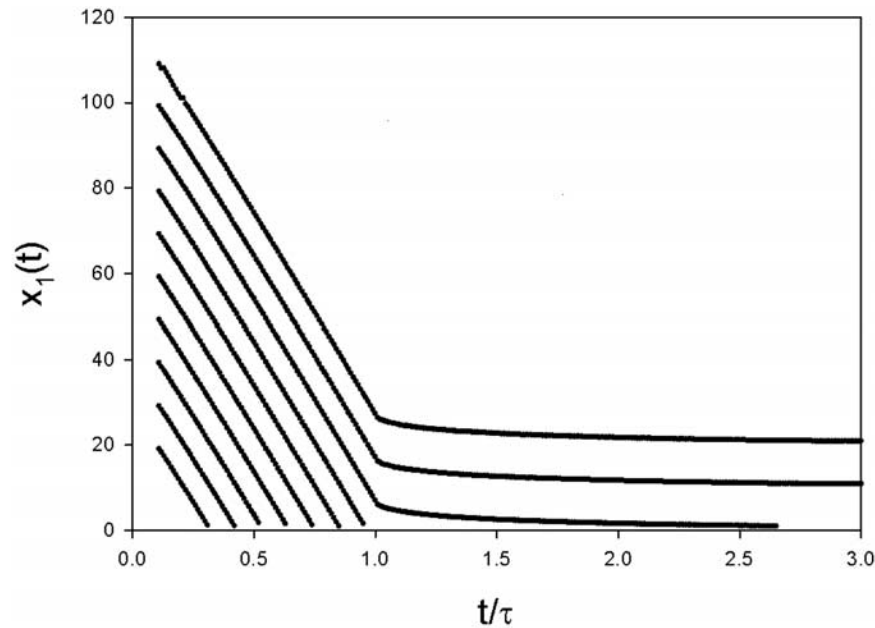


Figure 4. The same calculation as shown in Figure 3 but where the melt phase is slightly compressible (due, for example, to the presence of dissolved gas). This small but significant effect results in some degree of flow relaxation even after sucking has stopped. For example, calculated fluid trajectories in excess of 80 m distance can reach the channel but on a timescale slightly greater than $t/\tau = 2.6$.

243 question is, however, how far will a fluid element travel in
 244 the process? To answer this question, trajectories are calcu-
 245 lated. The actual fluid velocity in the plus region is $v(x,t)/n$,
 246 and, therefore, the location x_1 of a fluid element at time t
 247 that was initially at x_0 is

$$x_1(t) = x_0 + \int_0^t v(x_1(\bar{t}), \bar{t}) d\bar{t}. \quad (13)$$

Numerically, this formula is easily interpreted. The location 249
 difference at time t in a step dt is 250

$$x_1(t + dt) - x_1(t) = v(x_1(t), t) dt. \quad (14)$$

[16] The trajectories for this example are plotted in 253
 Figure 3. It is seen that during dilation ($t < \tau$) the velocity 254
 of a fluid element is almost constant. After the opening of the 255
 veins has ceased, the velocity becomes virtually zero. From 256

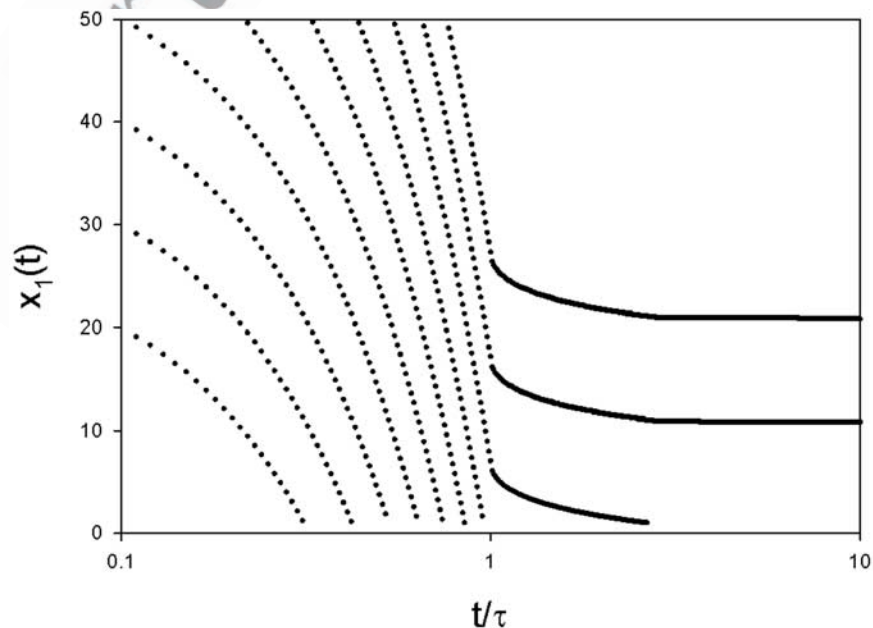


Figure 5. Trajectories as in Figure 4 but with a logarithmic time axis, emphasizing the effect of melt compressibility.

t2.1 **Table 2.** Values and Constants Used in the Analytical Model

t2.2	Process	Symbol	Value	Unit
t2.3	Channel opening volume strain	e_0	0.1	-
t2.4	Melt viscosity	η	1.0	Pa s
t2.5	Permeability of the channel region	k_0	10^{-8}	$\text{Pa}^{-1} \text{m}^2 \text{s}^{-1}$
t2.6	Matrix permeability	k	10^{-12}	$\text{Pa}^{-1} \text{m}^2 \text{s}^{-1}$
t2.7	Melt compressibility	β	10^{-10}	Pa^{-1}
t2.8	Shear strain in the zero region	γ	10^{-7}	s^{-1}
t2.9	Porosity of the channel region	n_0	0.4	-
t2.10	Matrix porosity (melt fraction)	n	0.001	-
t2.11	Half width of the channel region	δ	2	m
t2.12	Channel opening time	τ	10^7	s

257 this, it is concluded that fluid elements that complete their
 258 journey toward the central region within the time span $t < \tau$
 259 will arrive in the channelized region, while those that do not
 260 complete their journey in this period will not. The trajectories
 261 plotted in Figure 3 suggest that for the model parameters
 262 listed in Table 1, melt located within a radius of some 100 m
 263 of the channel zone will arrive there within the nondimen-
 264 sional timescale ($t/\tau = 1$). The melt flow velocity for this
 265 trajectory is $x_1(t)/\tau = 80 \text{ m}/3 \times 10^7 \text{ s} = 2.5 \times 10^{-6} \text{ m s}^{-1}$
 266 ($\sim 0.22 \text{ m a}^{-1}$). A fluid element located 110 m away will not
 267 make it to the channel unless the listed variables are
 268 changed. Sensitivity analysis suggests that matrix flow is
 269 relatively insensitive to matrix permeability.

270 [17] The same calculation is shown in Figure 4, this time
 271 for a melt phase that is slightly more compressible (due to the
 272 assumed presence of dissolved volatiles): $\beta = 10^{-9} \text{ Pa}^{-1}$.
 273 Here it is seen that for $t > \tau$ there is still a small velocity
 274 associated with the relaxation of the compressible melt. This
 275 would imply that fluid elements that cannot reach the “0”
 276 region in a time $t < \tau$ may still travel a short distance. A more
 277 careful study of this effect is depicted in Figure 5, where the
 278 timescale has been stretched by using a logarithmic scale. It
 279 is observed that the relaxation effect is confined to trajectories
 280 that were already close to the “0” region at time $t = \tau$.

281 [18] A sensitivity analysis is now carried out. Results are
 282 given in Table 1. We record the largest distance of a fluid
 283 element at time $t = 0$ that arrives at the center of the channel.
 284 All parameters are as in Table 2, except for the variation of
 285 one that is listed.

287 5. Discussion

288 5.1. Comparison With Melt Transport Models 289 Beneath Ridges

290 [19] For melt extraction in a subduction setting, the
 291 matrix downwelling velocity imposes a key timescale. For
 292 most subduction zones this is of the order $5\text{--}10 \text{ cm a}^{-1}$ (see
 293 compilation by *Plank and Langmuir* [1998]). Although
 294 decompression melting cannot be ruled out beneath some
 295 arcs [*Conder et al.*, 2002], by and large, arc mantle differs
 296 significantly from mid-ocean ridges and ocean islands in
 297 that the segregation process is coupled with the matrix
 298 upwelling velocity [*Stracke et al.*, 2003]. From the analysis
 299 given in section 3, the melt flow rate is circa 10^{-6} m s^{-1} ,
 300 3 orders of magnitude greater than average downwelling
 301 velocity, meaning that over the modeled transport time the
 302 matrix is effectively stationary and the model is fixed in the
 303 reference frame of the melt. A clear outcome of our analyt-
 304 ical calculations under model conditions is that average melt
 305 flow velocities lie at the upper end of those predicted at

constructive plate margins from numerical solutions. Chan- 306
 nel formation beneath ridge systems has been modeled 307
 successfully using a combination of compaction theory 308
 [McKenzie, 1985] and reactive fluid flow [e.g., *Spiegelman* 309
and Kelemen, 2003]. However, the estimated timescales for 310
 channel formation by reaction infiltration are 10^5 a^{-1} , far too 311
 long to preserve the observed U series disequilibria in arc 312
 magmas. Our melt transport model differs fundamentally 313
 from these and most other treatments (with the notable 314
 exception of that of *Ribe* [1986]) in that it deals with the 315
 lateral flow of melt, for which evidence exists from field 316
 studies of ophiolite complexes [e.g., *Abelson et al.*, 2001]. 317
 As we are not promoting buoyancy-driven flow, melt drawn 318
 into an opening channel is in principle free to flow toward it 319
 from any direction. On the basis of the illustrative values and 320
 constants listed in Table 2, the zone of influence surrounding 321
 a 2-m-wide dilating channel structure is 80 m. Keeping with 322
 this simple example but extending now to three dimensions, 323
 a volume $\sim 2 \times 10^9 \text{ L}$ of mantle rock could, in principle, be 324
 sampled by percolating melt moving toward a dilating 325
 channel on a characteristic timescale of 1 year. This is 326
 several times larger than the typical volumetric melting rate 327
 beneath arcs of $3 \times 10^{-4} \text{ km}^3 \text{ a}^{-1}$, implying that the sucking 328
 effect could operate on length scales that are significant with 329
 respect to typical magma production rates. The potential 330
 sample volume will be clearly larger if the model timescale 331
 (τ) is increased. Should the source region comprise 332
 numerous, closely spaced channels (similar arrangements 333
 beneath mid-ocean ridges suggest spacings of a meter to 334
 several hundred meters [*Kelemen and Dick*, 1995]), then 335
 conceptually we can imagine a situation where melt is 336
 sucked toward channels which have overlapping radii of 337
 influence. Should the mantle wedge be chemically hetero- 338
 geneous on a scale comparable with the melt transport 339
 distance, governed largely by the channel opening rate, the 340
 opportunity exists to impart chemical variation in the melt 341
 phase at source as it migrates toward and into a dilating 342
 channel. While a full exploration of the geochemical con- 343
 sequences on melt composition entering a channel lie outside 344
 the scope of this study, it should be noted that lateral flow has 345
 the potential to introduce subtle and potentially complex 346
 chemical variations in trace element and isotopic composi- 347
 tions of melts in the source region that may not be apparent 348
 in models based purely on gravity-driven flow. 349

5.2. Speculations on Channel Formation in Downwelling Mantle Wedge

350
 351
 352 [20] Implicit in the modeling is that channels with indi- 352
 vidualy dilating veins can actually form in the source 353
 region. But how might this happen in reality? Arguably, 354
 there should be some link between partial melting and 355
 channel formation (similar arguments hold sway in the 356
 continental crust [see *Brown and Rushmer*, 1997, and 357
 references therein]), but this link is not obvious in mantle 358
 rocks. For example, while partial melting has been shown to 359
 result in volume changes sufficient in magnitude to induce 360
 cracking in ductile media [*Rushmer*, 2001], the general 361
 outcome of this process is to push fluid out of the rock 362
 [e.g., *Murton et al.*, 2006] not to suck it in as argued here. It, 363
 thus, seems that thermal stresses associated with partial 364
 melting are unlikely to be the primary cause of dilation in 365
 this instance. 366

[21] The alternative is to appeal to tectonic deformation. It has been noted that the interface between the downwelling slab and overriding mantle wedge is a type of shear zone [e.g., *van Keken*, 2003] resulting in localized, high-temperature viscous deformation. If an elliptical object is simply sheared with shear strain γ , the volume strain is of the order of γ^2 . This direct “mean field” approach would imply that the volume strain rate is a second-order effect. This is not so when an inclusion-type theory for elliptical inclusions in an elastic medium (ideal mantle matrix) is considered. Formulas for this are available [*Walpole*, 1977]. Here no full calculations are given, but if the formulae are made relevant to an elliptical channel aligned with major principal direction of the shear direction, the volume strain is of the order of magnitude of the shear strain γ for a channel in which the major principal axis is much greater than the minor principal axis. Thus, it follows that the rate of shear required to drive the process envisaged here must be of the order of magnitude of 10^{-7} s^{-1} if the zone marked zero (Figure 1) has a vein concentration of some 10%. Such a rate of shearing is clearly much larger than the mean tectonic background value. The tentative implication is that during subduction, localized zones of dilation leading to channel formation will only occur at higher-than-average (plate tectonic) strain rates. However, the model still requires that melting, or a melt phase, is located within sucking distance of an opening channel. In standard iso-viscous mantle models, the zone of partial melting is restricted to a confined region located above and away from the slab top. However, thermal models based on a non-Newtonian rheology focus heat (and by implication partial melting) much closer to the slab mantle interface where viscous deformation is also most likely to be strongest [e.g., *Cagnioncle et al.*, 2007]. Thus, a qualitative picture, underpinned in part by robust physics, emerges whereby channels in the wedge melting zone form because of stresses and draw toward them contemporaneous partial melt from their surroundings as they progressively dilate. Arc mantle with non-Newtonian rheology appears to offer the most convenient way of collocating the essential ingredients of partial melt and shearing in the mantle wedge such that channels of the kind described here can form in the source region.

5.3. Implications for U Series Disequilibria in Arc Magmas

[22] Whatever the finer details of variability in melt composition resulting from radial flow and the mechanism responsible for rapid lithospheric-scale transport of melt to the surface turn out to be, the implications for preserving isotopic disequilibria in arc magmas at source now become clearer. Given the parameters outlined in section 3, small-scale porous flow into veins or channels located in the mantle source region is easily fast enough to preserve excess ^{226}Ra . More controversially, our modeled melt transport times at relevant melt fractions (10^{-3}) are less than the ^{210}Pb half-life of 22.5 years. This raises the theoretical possibility that some ^{210}Pb deficits in arc lavas reflect fractionation during partial melting rather than late stage contrasts in gas and magma transport beneath the volcanic edifice [*Turner et al.*, 2004]. A similar conclusion was reached by *Rubin et al.* [2005b], who used ^{210}Pb deficits in mid-ocean ridge basalts to argue for ultrarapid

melt extraction rates of less than a decade. Our results suggest that lateral porous media flow on the decimeter scale, driven by relatively modest pressure gradients, is consistent with the idea that short-lived isotope disequilibria in some arc magmas would permit melting at source.

[23] In the arc environment this is, in principle, testable by obtaining further ^{210}Pb data on primitive lavas and looking for correlations with indices of fluid addition or other melting signals such as ^{235}U - ^{231}Pa disequilibria. Moreover, if ^{231}Pa - ^{227}Ac disequilibria were found in arc lavas, this would prove that melting-induced disequilibria formed on the decadal timescale can be preserved since unlike ^{226}Ra - ^{210}Pb , there is no gaseous intermediate in this system to offer an alternative explanation. While both of these tests must await further data collection, it is worthwhile considering the ramifications of these timescales for melt segregation if applicable. The most obvious is that measured ^{226}Ra excesses would be primary and unaffected by decay in any lavas shown to preserve a source ^{210}Pb (or ^{227}Ac) signal. First, ^{230}Th - ^{226}Ra disequilibria is primarily a function of residual porosity in the melting region, and this could, in principle, be quantified, removing a key unknown in all ingrowth melting models. Second, as ^{226}Ra excesses are frequently thought to derive from the base of the arc melting column, tighter constraints on melt ascent would be possible, and these may rule out models invoking significant melt-wall rock interaction during magma passage. Third, the commonly observed decreases in ($^{226}\text{Ra}/^{230}\text{Th}$) with increasing extent of differentiation would no longer constrain the timescales of differentiation but rather would require a major role for amphibole during fractionation. Evidence for this has been emerging [*Davidson et al.*, 2007]. Instead, differentiation would have to occur on the decadal timescale and, thus, be similar to eruptive periodicity. This might reconcile some very young ages from diffusion studies (see review by *Turner and Costa* [2007]) and would require that differentiation occur during magma ascent and be strongly controlled by decompression [e.g., *Blundy and Cashman*, 2001] rather than just crystallization due to cooling alone.

Appendix A

[24] Three regions are distinguished (Figure 1): zero, where the veins comprising the high-permeability channel are located; plus, almost undeformable permeable material to the right of zero at $x > \delta$; and minus, almost undeformable permeable material to the left of 0 at $x < -\delta$. The flow is driven by a strain that is ramped up to a value e_0 in a time τ . For $t > \tau$ the strain is constant at e_0 .

[25] Biot’s equation reads

$$k_0 \frac{\partial^2 p}{\partial x^2} = n_0 \beta \frac{\partial p}{\partial t} + \frac{\partial e}{\partial t} \quad (-\delta < x < \delta) \quad (\text{A1})$$

$$k \frac{\partial^2 p}{\partial x^2} = n \beta \frac{\partial p}{\partial t} \quad (x > \delta, x < -\delta). \quad (\text{A2})$$

[26] The boundary conditions are

$$p(\delta - \varepsilon, t) = p(\delta + \varepsilon, t) \quad (\varepsilon \rightarrow 0), \quad (\text{A3})$$

$$p(-\delta - \varepsilon, t) = p(-\delta + \varepsilon, t) \quad (\varepsilon \rightarrow 0), \quad (\text{A4})$$

487

$$k_0 \frac{\partial p}{\partial x}(\delta - \varepsilon, t) = k \frac{\partial p}{\partial x}(\delta + \varepsilon, t) \quad (\varepsilon \rightarrow 0), \quad (\text{A5})$$

488

$$k_0 \frac{\partial p}{\partial x}(-\delta + \varepsilon, t) = k \frac{\partial p}{\partial x}(-\delta - \varepsilon, t) \quad (\varepsilon \rightarrow 0), \quad (\text{A6})$$

$$\frac{\partial p}{\partial x}(\pm L, t) = 0 \quad (L \rightarrow \infty). \quad (\text{A7})$$

493 [27] The solution is obtained by Laplace transform with
495 Laplace frequency s :

$$k_0 \frac{\partial^2 \hat{p}}{\partial x^2} = n_0 \beta s \hat{p} + s \hat{e} \quad (-\delta < x < \delta) \quad (\text{A8})$$

$$k \frac{\partial^2 \hat{p}}{\partial x^2} = n \beta s \hat{p} \quad (x > \delta, x < -\delta). \quad (\text{A9})$$

500 [28] The solution is for the minus region,

$$\hat{p} = \frac{\hat{e} k_0 \mu_0 e^{\mu(x+\delta)\sqrt{s}} (1 - e^{2\mu_0\delta\sqrt{s}})}{\beta n_0 (e^{2\mu_0\delta\sqrt{s}}(k\mu + k_0\mu_0) + k\mu - k_0\mu_0)}, \quad (\text{A10})$$

501 zero region,

$$\hat{p} = \frac{\hat{e} k \mu [e^{\mu_0(x+\delta)\sqrt{s}} + e^{\mu_0(-x+\delta)\sqrt{s}}]}{\beta n_0 (e^{2\mu_0\delta\sqrt{s}}(k\mu + k_0\mu_0) + k\mu - k_0\mu_0)}, \quad (\text{A11})$$

504 and plus region,

$$\hat{p} = \frac{\hat{e} k_0 \mu_0 e^{\mu(-x+\delta)\sqrt{s}} (1 - e^{2\mu_0\delta\sqrt{s}})}{\beta n_0 (e^{2\mu_0\delta\sqrt{s}}(k\mu + k_0\mu_0) + k\mu - k_0\mu_0)}, \quad (\text{A12})$$

506 where $\mu_0 = \sqrt{n_0\beta/k_0}$ and $\mu = \sqrt{n\beta/k}$.

507 [29] The superficial velocity is obtained from

$$v = -k \frac{\partial p}{\partial x}. \quad (\text{A13})$$

508 So, the minus region is

$$\hat{v} = -\frac{\hat{e} k k_0 \mu_0 \sqrt{s} e^{\mu(x+\delta)\sqrt{s}} (1 - e^{2\mu_0\delta\sqrt{s}})}{\beta n_0 (e^{2\mu_0\delta\sqrt{s}}(k\mu + k_0\mu_0) + k\mu - k_0\mu_0)}, \quad (\text{A14})$$

510 zero region is

$$\hat{v} = \frac{\hat{e} k^2 \mu \sqrt{s} [\mu_0 e^{\mu_0(x+\delta)\sqrt{s}} - e^{\mu_0(-x+\delta)\sqrt{s}}]}{\beta n_0 (e^{2\mu_0\delta\sqrt{s}}(k\mu + k_0\mu_0) + k\mu - k_0\mu_0)}, \quad (\text{A15})$$

513 and plus region is

$$\hat{v} = \frac{\hat{e} k k_0 \mu_0 \sqrt{s} e^{\mu(-x+\delta)\sqrt{s}} (1 - e^{2\mu_0\delta\sqrt{s}})}{\beta n_0 (e^{2\mu_0\delta\sqrt{s}}(k\mu + k_0\mu_0) + k\mu - k_0\mu_0)}.$$

A1. Solution in the Plus Region

515

[30] The inverse Laplace transform in the plus region is
obtained as follows: 516
517

$$\begin{aligned} \hat{e} &= \frac{k_0 \mu_0}{\beta n_0 (k\mu + k_0\mu_0)} \frac{e^{\mu(-x+\delta)\sqrt{s}} (e^{-2\mu_0\delta\sqrt{s}} - 1)}{\left(1 + \frac{k\mu - k_0\mu_0}{k\mu + k_0\mu_0} e^{-2\mu_0\delta\sqrt{s}}\right)} \\ &= \hat{e} \frac{k_0 \mu_0 e^{\mu(-x+\delta)\sqrt{s}} (e^{-2\mu_0\delta\sqrt{s}} - 1)}{\beta n_0 (k\mu + k_0\mu_0)} \sum_{j=0}^{\infty} \left(\frac{-k\mu + k_0\mu_0}{k\mu + k_0\mu_0}\right)^j e^{-2j\mu_0\delta\sqrt{s}}. \end{aligned}$$

518 [31] Now, a slightly more general approach is taken. First,
519 note that 521

$$\mathfrak{F}^{-1}(e^{-\zeta\sqrt{s}}) = \frac{\zeta}{2\sqrt{\pi t^3}} e^{-\zeta^2/(4t)}$$

and 522

$$\mathfrak{F}^{-1}(\hat{e}) = e_0 \frac{t}{\tau} (t < \tau) = e_0 (t > \tau), \quad (\text{A17})$$

so,

$$\mathfrak{F}^{-1}(\hat{e} e^{-\zeta\sqrt{s}}) = \int_0^t e_0 \frac{(t-\lambda)}{\tau} \frac{\zeta}{2\sqrt{\pi\lambda^3}} e^{-\zeta^2/(4\lambda)} (t < \tau)$$

$$= \int_{t-\tau}^t e_0 \frac{(t-\lambda)}{\tau} \frac{\zeta}{2\sqrt{\pi\lambda^3}} e^{-\zeta^2/(4\lambda)}$$

$$+ \int_0^{t-\tau} e_0 \frac{\zeta}{2\sqrt{\pi\lambda^3}} e^{-\zeta^2/(4\lambda)} (t > \tau). \quad (\text{A18})$$

[32] The integrals are easily done, and the outcome is 526

$$\begin{aligned} \mathfrak{F}^{-1}(\hat{e} e^{-\zeta\sqrt{s}}) &= -\frac{e_0 \zeta \sqrt{t} \exp\left(-\frac{\zeta^2}{4t}\right)}{\tau \sqrt{\pi}} + \frac{e_0 (2t + \zeta^2) \left[1 - \operatorname{erf}\left(\frac{\zeta}{2\sqrt{t}}\right)\right]}{2\tau} (t < \tau) \\ &= e_0 + \frac{e_0 \zeta \left(\exp\left(\frac{-\zeta^2}{4(t-\tau)}\right) \sqrt{t-\tau} - \exp\left(\frac{-\zeta^2}{4t}\right) \sqrt{t}\right)}{\tau \sqrt{\pi}} \\ &= \frac{e_0 \left[(2t - 2\tau + \zeta^2) \operatorname{erf}\left(\frac{\zeta}{2\sqrt{t-\tau}}\right) - (2t + \zeta^2) \operatorname{erf}\left(\frac{\zeta}{2\sqrt{t}}\right) \right]}{2\tau} \\ &\quad \cdot (t > \tau). \quad (\text{A19}) \end{aligned}$$

[33] Call $\hat{\Psi}_0 e_0 \equiv \mathfrak{F}^{-1}(\hat{e} e^{-\zeta\sqrt{s}})$, then the following
hierarchy is generated: 531
532

$$\begin{aligned} \hat{\Psi}_1(s, \zeta) e_0 &= \mathfrak{F}^{-1}(\hat{e} \sqrt{s} e^{-\zeta\sqrt{s}}) = -\frac{\partial}{\partial \zeta} \mathfrak{F}^{-1}(\hat{e} e^{-\zeta\sqrt{s}}), \\ \hat{\Psi}_2(s, \zeta) e_0 &= \mathfrak{F}^{-1}(\hat{e} s e^{-\zeta\sqrt{s}}) = \frac{\partial^2}{\partial \zeta^2} \mathfrak{F}^{-1}(\hat{e} e^{-\zeta\sqrt{s}}), \quad (\text{A20}) \end{aligned}$$

534 [34] In the time domain, the differentiations with respect
536 to ζ yield the following:

$$\begin{aligned} \Psi_1(\zeta, t) &= \frac{2\sqrt{t} \exp\left(-\frac{\zeta^2}{4t}\right)}{\tau\sqrt{\pi}} - \frac{\zeta \left[1 - \operatorname{erf}\left(\frac{\zeta}{2\sqrt{t}}\right)\right]}{\tau} \quad (t < \tau) \\ &= -\frac{2\left(\exp\left(\frac{-\zeta^2}{4(t-\tau)}\right)\sqrt{t-\tau} - \exp\left(\frac{-\zeta^2}{4t}\right)\sqrt{t}\right)}{\tau\sqrt{\pi}} \\ &\quad - \frac{\zeta \left[\operatorname{erf}\left(\frac{\zeta}{2\sqrt{t-\tau}}\right) - \operatorname{erf}\left(\frac{\zeta}{2\sqrt{t}}\right)\right]}{\tau} \quad (t > \tau), \end{aligned} \quad (\text{A21})$$

$$\begin{aligned} \Psi_2(\zeta, t) &= \frac{\zeta \left[1 - \operatorname{erf}\left(\frac{\zeta}{2\sqrt{t}}\right)\right]}{\tau} \quad (t < \tau) \\ &= \frac{\zeta \left[\operatorname{erf}\left(\frac{\zeta}{2\sqrt{t-\tau}}\right) - \operatorname{erf}\left(\frac{\zeta}{2\sqrt{t}}\right)\right]}{\tau} \quad (t > \tau), \end{aligned} \quad (\text{A22})$$

$$\begin{aligned} \Psi_3(\zeta, t) &= \frac{\exp\left(-\frac{\zeta^2}{4t}\right)}{\tau\sqrt{\pi t}} \quad (t < \tau) \\ &= \frac{\exp\left(-\frac{\zeta^2}{4t}\right)}{\tau\sqrt{\pi t}} - \frac{\exp\left(-\frac{\zeta^2}{4(t-\tau)}\right)}{\tau\sqrt{\pi(t-\tau)}} \quad (t > \tau), \end{aligned} \quad (\text{A23})$$

$$\begin{aligned} p(x, t) &= \frac{e_0 k_0 \mu_0}{\beta n_0 (k\mu + k_0 \mu_0)} \sum_{j=0}^{\infty} \left(\frac{-k\mu + k_0 \mu_0}{k\mu + k_0 \mu_0}\right)^j \\ &\quad \cdot [\Psi_0(\mu(x-\delta) + 2(j+1)\mu_0\delta, t) \\ &\quad - \Psi_0(\mu(x-\delta) + 2j\mu_0\delta, t)], \end{aligned} \quad (\text{A24})$$

$$\begin{aligned} v(x, t) &= -\frac{e_0 k k_0 \mu_0 \mu}{\beta n_0 (k\mu + k_0 \mu_0)} \sum_{j=0}^{\infty} \left(\frac{-k\mu + k_0 \mu_0}{k\mu + k_0 \mu_0}\right)^j \\ &\quad \cdot [\Psi_1(\mu(x-\delta) + 2(j+1)\mu_0\delta, t) \\ &\quad - \Psi_1(\mu(x-\delta) + 2j\mu_0\delta, t)]. \end{aligned} \quad (\text{A25})$$

547 A2. Long Time Approximation

548 [35] For long times, that is for $t \gg 4(\mu_0\delta)^2$, the formulas
549 may be approximated. In the plus region,

$$\hat{p} = \hat{e} e^{\mu(-x+\delta)\sqrt{s}} \left(\frac{\delta\sqrt{s}}{\sqrt{\beta nk}} - \frac{\delta^2 n_0 s}{nk} \right), \quad (\text{A26})$$

$$\hat{v} = \hat{e} e^{\mu(-x+\delta)\sqrt{s}} \left(-\delta s + \delta^2 n_0 s^{3/2} \sqrt{\frac{\beta}{nk}} \right). \quad (\text{A27})$$

552 In the time domain, these become

$$p(x, t) = -\frac{e_0 \delta}{\sqrt{\beta nk}} \Psi_1(\mu(x-\delta), t) + \frac{e_0 \delta^2 n_0}{nk} \Psi_2(\mu(x-\delta), t) \quad (\text{A28})$$

$$v(x, t) = -e_0 \delta \Psi_2(\mu(x-\delta), t) + e_0 \delta^2 n_0 \Psi_3(\mu(x-\delta), t). \quad (\text{A29})$$

[36] **Acknowledgments.** N.P. would like to thank Macquarie University and the Royal Society, London, for financial support. S.T. acknowledges the ARC for a Federation Fellowship. Craig Lundstrom and an anonymous reviewer are thanked for helpful comments. 558
559
560
561

References

- 562
Abelson, M., G. Baer, and A. Agnon (2001), Evidence from gabbro of the 563
Troodos ophiolite for lateral magma transport along a slow-spreading 564
mid-ocean ridge, *Nature*, *409*, 72–75. 565
Aharonov, E., J. A. Whitehead, P. B. Kelemen, and M. Spiegelman (1995), 566
Channeling instability of upwelling melt in the mantle, *J. Geophys. Res.*, 567
100, 20,433–20,450. 568
Asimow, P. D., and E. M. Stolper (1999), Steady state mantle–melt inter- 569
actions in one dimension: 1. Equilibrium transport and melt focusing, 570
J. Petrol., *40*, 475–494. 571
Blundy, J., and K. Cashman (2001), Ascent-driven crystallisation of dacite 572
magmas at Mount St Helens, 1980–1986, *Contrib. Mineral. Petrol.*, *140*, 573
631–650. 574
Bourdon, B., S. Turner, and N. M. Ribe (2005), Partial melting and upwel- 575
ling rates beneath the Azores from a U-series isotope perspective, *Earth 576
Planet. Sci. Lett.*, *239*, 42–56. 577
Brown, M., and T. Rushmer (1997), The role of deformation in the 578
movement of granitic melt: Views from the laboratory and the field, in 579
Deformation-Enhanced Fluid Transport in the Earth's Crust and Mantle, 580
edited by M. B. Holness, pp. 111–139, Chapman and Hall, London. 581
Cagnioncle, A.-M., E. M. Parmentier, and L. T. Elkins-Tanton (2007), 582
Effect of solid flow above a subducting slab on water distribution and 583
melting at convergent boundaries, *J. Geophys. Res.*, *112*, B09402, 584
doi:10.1029/2007JB004934. 585
Conder, J. A., D. A. Wiens, and J. Morris (2002), On the decompression 586
melting structure at volcanic arcs and back-arc spreading centers, in 587
Geophys. Res. Lett., *29*(15), 1727, doi:10.1029/2002GL015390. 588
Davidson, J., S. Turner, A. Dosseto, and H. Handley (2007), Amphibole 589
sponge in arc crust?, *Geology*, *35*, 787–790. 590
Huang, F., and C. C. Lundstrom (2007), ²³¹Pa excesses in arc volcanic 591
rocks: Constraints on melting rates at convergent margins, *Geology*, *35*, 592
1007–1010. 593
Kelemen, P. B., and H. J. B. Dick (1995), Focused melt flow and localized 594
deformation in the upper mantle: Juxtaposition of replacive dunite and 595
ductile shear zones in the Josephine peridotite, SW Oregon, *J. Geophys.* 596
Res., *100*, 423–438. 597
Maaloe, S. (2005), Extraction of melt from veined mantle source regions 598
during eruptions, *J. Volcanol. Geotherm. Res.*, *147*, 377–390. 599
McKenzie, D. (1985), ²³⁰Th–²³⁸U disequilibrium and the melting process 600
beneath ridge axes, *Earth Planet. Sci. Lett.*, *72*, 149–157. 601
Murton, J. B., R. Peterson, and J.-C. Ozouf (2006), Bedrock fracture by ice 602
segregation in cold regions, *Science*, *314*, 1127–1129. 603
Plank, T., and C. H. Langmuir (1998), The chemical composition of 604
subducting sediment and its consequences for the crust and mantle, 605
Chem. Geol., *145*, 325–394. 606
Ribe, N. M. (1986), Melt segregation driven by dynamic forcing, *Geophys.* 607
Res. Lett., *13*, 1462–1465. 608
Rubin, K. H., I. van der Zander, M. C. Smith, and E. C. Bergmanis (2005a), 609
²¹⁰Pb, ²²⁶Ra–²³⁰Th disequilibria in very young mid-ocean ridge basalts, 610
Geochim. Cosmochim. Acta, *69*, A338. 611
Rubin, K. H., I. van der Zander, M. C. Smith, and E. C. Bergmanis (2005b), 612
New speed limit for ocean ridge magmatism, *Nature*, *437*, 534–538. 613
Rushmer, T. (2001), Volume change during partial melting reactions: 614
Implications for melt extraction, melt geochemistry and crustal rheology, 615
Tectonophysics, *342*, 389–405. 616
Sleep, N. H. (1988), Tapping melts by veins and dykes, *J. Geophys. Res.*, 617
93, 10,225–10,272. 618
Spiegelman, M., and T. Elliott (1993), Consequences of melt transport for 619
uranium series disequilibrium, *Earth Planet. Sci. Lett.*, *118*, 1–20. 620
Spiegelman, M., and P. B. Kelemen (2003), Extreme chemical variability as 621
a consequence of channelized melt transport, *Geochem. Geophys. Geosyst.*, 622
4(7), 1055, doi:10.1029/2002GC000336. 623
Spiegelman, M., P. B. Kelemen, and E. Aharonov (2001), Causes and 624
consequences of flow organization during melt transport: The reaction 625
infiltration instability in compactible media, *J. Geophys. Res.*, *106*, 626
2061–2077. 627
Stevenson, D. J. (1989), Spontaneous small scale melt segregation in partial 628
melts undergoing deformation, *Geophys. Res. Lett.*, *16*, 1067–1070. 629
Stracke, A., A. Zindler, V. J. M. Salters, D. McKenzie, and K. Groendvold 630
(2003), The dynamics of melting beneath Theistareykir, northern Iceland, 631
Geochem. Geophys. Geosyst., *4*(10), 8513, doi:10.1029/2002GC000347. 632
Stracke, A., B. Bourdon, and D. McKenzie (2006), Melt extraction in the 633
Earth's mantle: Constraints from U–Th–Pa–Ra studies in oceanic basalts, 634
Earth Planet. Sci. Lett., *244*, 97–112. 635

- 636 Takahashi, N. (1992), Evidence for melt segregation toward fractures in the
637 Horoman mantle peridotite complex, *Nature*, 359, 52–55.
- 638 Turner, S., and F. Costa (2007), Measuring timescales of magmatic evolu-
639 tion, *Elements*, 3, 267–273.
- 640 Turner, S., P. Evans, and C. Hawkesworth (2001), Ultra-fast source-to-
641 surface movement of melt at island arcs from ^{226}Ra - ^{230}Th systematics,
642 *Science*, 292, 1363–1366.
- 643 Turner, S., B. Bourdon, and J. Gill (2003), Insights into magma genesis
644 at convergent margins from U-series isotopes, in *Uranium-Series*
645 *Geochemistry*, *Rev. Mineral. Geochem.*, vol. 52, edited by B. Bourdon,
646 et al., pp. 255–315., Mineral. Soc. of Am., Washington, D. C.
- 647 Turner, S., S. Black, and K. Berlo (2004), ^{210}Pb - ^{226}Ra and ^{228}Ra - ^{232}Th
648 systematics in young arc lavas: Implications for magma degassing and
649 ascent rates, *Earth Planet. Sci. Lett.*, 227, 1–16.
- 650 Turner, S., M. Regelous, C. Hawkesworth, and K. Rostami (2006), Partial
651 melting processes above subducting plates: Constraints from ^{231}Pa - ^{235}U
652 disequilibria, *Geochim. Cosmochim. Acta*, 70, 480–503.
- van Keken, P. E. (2003), The structure and dynamics of the mantle wedge, 653
Earth Planet. Sci. Lett., 215, 323–338. 654
- Walpole, L. J. (1977), The determination of the elastic field of an ellipsoidal 655
inclusion in an anisotropic medium, *Math. Proc. Cambridge Philos. Soc.*, 656
81, 283–289. 657
- Williams, R. W., and J. B. Gill (1989), Effects of partial melting on the 658
uranium decay series, *Geochim. Cosmochim. Acta*, 53, 1607–1619. 659
-
- M. A. Koenders, Centre for Earth and Environmental Science Research, 661
Kingston University, Penrhyn Road, Kingston-upon-Thames KT1 2EE, UK. 662
- N. Petford, School of Conservation Sciences, Bournemouth University, 663
Talbot Campus, Fern Barrow, Poole BH12 5BB, UK. (npetford@ 664
bournemouth.ac.uk) 665
- S. Turner, GEMOC, Department of Earth and Planetary Sciences, 666
Macquarie University, Sydney, NSW 2109, Australia. 667

Article in Proof